JOURNAL OF GEOPHYSICAL RESEARCH, VOL. ???, XXXX, DOI:10.1029/,

Global Autocorrelation Scales of the Partial Pressure of Oceanic CO_2

Zhen Li,[1] David Adamec,[2] Taro Takahashi and Stewart C. Sutherland[3]

[1]Science Applications International

Corporation, Beltsville, MD, USA

[2]Oceans and Ice Branch, NASA/GSFC,

Greenbelt, MD, USA.

[3]Lamont-Doherty Earth Observatory,

Palisades, NY, USA.

Abstract. A global database of approximately 1.7 million observations of the partial pressure of carbon dioxide in surface ocean waters (pCO_2) collected between 1970 and 2003 is used to estimate its spatial autocorrelation structure. The patterns of the lag distance where the autocorrelation exceeds 0.8 is similar to patterns in the spatial distribution of the first baroclinic Rossby radius of deformation indicating that ocean circulation processes play a significant role in determining the spatial variability of pCO_2. For example, the global maximum of the distance at which autocorrelations exceed 0.8 averages about 140 km in the equatorial Pacific. Also, the lag distance at which the autocorrelation exceed 0.8 is greater in the vicinity of the Gulf Stream than it is near the Kuroshio, approximately 50km near the Gulf Stream as opposed to 20 km near the Kuroshio. Separate calculations for times when the sun is north and south of the equator revealed no obvious seasonal dependence of the spatial autocorrelation scales. The pCO_2 measurements at Ocean Weather Station (OWS) "P" in the eastern subarctic Pacific (50°N, 145°W) is the only fixed location where an uninterrupted time series of sufficient length exists to calculate a meaningful temporal autocorrelation function for lags greater than a few days. The estimated temporal autocorrelation function at OWS "P" is highly variable. A spectral analysis of the longest four pCO_2 time series indicates a high level of variability occurring over periods from the atmospheric synoptic to the maximum length of the time series, in this case 42 days. It is likely that a relative peak in variability with a period of 3-6 days is related to atmospheric synoptic period variability and

ocean mixing events due to wind stirring. However, the short length of available time series makes identifying temporal relationships between pCO_2 and atmospheric or ocean processes problematic.

1. INTRODUCTION

The partial pressure of CO_2 (pCO_2) in seawater is a vapor pressure of CO_2, and hence governs the magnitude of the CO_2 transfer flux across the sea-air interface when multiplied with sea-air gas transfer coefficient. It is a sensitive function of temperature doubling with every 16 °C (Takahashi *et al.*, 1993). It is also a sensitive function of the total concentration of CO_2 (TCO_2) species dissolved in seawater

$$TCO_2 = [CO_2]_{aqueous} + HCO_3^- + CO_3^{--}$$

that depends on the net biological community production, the rate of upwelling of subsurface waters rich in CO_2, and the air-sea CO_2 flux. The local sensitivity may be expressed in terms of the Revelle factor, $\frac{\partial lnpCO_2}{\partial lnTCO_2}$, which varies from 8 with lower TCO_2 concentrations in tropical waters to 15 with higher concentrations in polar waters. In the surface mixed layer, the effect of warming on pCO_2 is counteracted by lower TCO_2 caused by photosynthetic fixation of CO_2, as often seen during spring bloom periods; and the effect of cooling is counteracted by increasing TCO_2 usually caused by upwelling of subsurface waters rich in respired CO_2. Consider the following example. A parcel of polar ocean water at -1.9 °C warmed to an equatorial temperature of 30°C without changes in TCO_2 and other chemicals, increases its pCO_2 by a factor of 4. If the typical nitrate in this water ($\sim$35 μmol/kg) is completely utilized by biological growth with the Redfield N/C ratio of 16/106, then the TCO_2 in the same water would decrease from 2150 μmol/kg to 1920 μmol/kg. Thus, there is a decrease in pCO_2 by a factor of $(1920/2150)^{10} \approx 33\%$ (using a Revelle factor of 10). This example illustrates that, over the global oceans, the effect of change in temperature is roughly compensated by changes in TCO_2, and that the

time-space variation in surface seawater pCO_2 is dictated primarily by interactions between the effects of temperature, net biological production and the deep water upwelling rate. Using climatological mean data, Takahashi *et al.* (2002) have observed that, in subtropical gyres, seasonal changes in pCO_2 are due primarily to temperature changes, whereas those in sub-polar and polar waters are due primarily to TCO_2 changes caused by winter upwelling of subsurface waters and spring plankton blooms in spring. However, finer scale time-space variability of surface water pCO_2 has not been investigated using semi-continuous underway surface water pCO_2 measurements which have been made in increasing numbers during recent years.

In this study, the global distribution of the isotropic spatial autocorrelation structure of available pCO_2 underway measurements is calculated. The motivation is to identify the scales of variability that are resolved in the pCO_2 data, and attempt to relate some of that variability to known physical processes. In addition, time series data available from OWS "P" is similarly analyzed to provide an example of temporal autocorrelation structure and variability. It is hoped that a quantified estimate of autocorrelation scales will be useful to investigators, particularly future data assimilation efforts, for decisions on how best to use the 1.7 million measurements in choosing averaging and sub-sampling schemes for their work.

2. DATA

For the global studies, most of the pCO_2 measurements in surface mixed layer waters (hereafter referred to simply as pCO_2) are mostly comprised of underway shipboard measurements and a much smaller number of measurements for discrete water samples collected at hydrographic stations. The underway data used for both Takahashi *et al.*

(1997, 2002) studies was temporally averaged to 12-hourly intervals; the averaging reducing the number of total observations as underway measurements in the complete data set are sometimes taken as frequently as every 2 minutes, but usually several times per hour. The 12-hourly (approximately 100 km) averaging period was chosen ostensibly to maintain the larger scale gradient structure of pCO_2 in the total data set.

While the raw number of pCO_2 measurements (currently approaching 1.7 million in some data sets) may seem adequate, or perhaps even large, for global studies, the number of actual data values used in past studies is much lower because of the averaging of the underway data as noted above. Even the choice of averaging period/distance is, in some ways, an *ad hoc* choice depending on the scales of interest and the accuracy of underway data versus station point data. Indeed, the relative paucity of accurate pCO_2 measurements has lead some investigators to try to infer pCO_2 values from other properties of the seawater, such as temperature. For example, Boutin *et al.* (1999) and Feely *et al.* (2004) found strong co-variability between pCO_2 and sea surface temperature in the equatorial Pacific, and Loukos *et al.* (2000) were able to show a useful predictive skill of temperature and salinity for TCO_2 in the equatorial Pacific.

The pCO_2 data used here is an expanded version of the data used in Takahashi *et al.* (2002), including about 760,000 new observations bringing the total to approximately 1.7 million. The data was collected between 1970 and 2003, and its geographic and rough temporal distributions are shown in Fig. 1. Note, for the most part, the entire Indian and South Pacific Oceans are only sparsely sampled prior to 1990. Much of the sampling in the South Atlantic occurred between 1985 and 1989. Prior to 1985, the only sub basin

that is sampled more densely is the North Atlantic. A caution on the results presented here is that the results apply to sampling that primarily took place post 1984.

All autocorrelation calculations are performed on data interpolated to regularly spaced segments with a distance of 2 km between successive data points. Interpolating pCO_2 data across gaps larger than 20 km is not done. For gaps larger than 20 km, a new segment is defined. Also, interpolation across a gap in time of longer than 10 days is not allowed, and a new segment would be defined. This latter condition was very rarely met. Average autocorrelation functions are calculated globally on a 10^o x 10^o grid. The location of the segment is taken to be the average latitude and longitude of the measurement locations. Segments shorter than 60 km were not included in the calculations, and no single segment was allowed to exceed 1000 km, approximately the length of the grid box. For segments longer than 1000 km, a group of subsegments, broken every 1000 km, was used for the calculations. Thus, the autocorrelations describe variability on approximate spatial scales less than the grid box resolution.

The global distribution of segments is not homogeneous, and the number of segments in each grid box is presented in Fig. 2. Areas of densest coverage include the tropical Pacific, the North Pacific near the coast of Japan and north of 45^oN, the northwest Indian Ocean, the Caribbean and specific locales in the Southern Ocean. In many places, the correlations presented are the result from only 1 or 2 segments, such as is the case for much of the South Atlantic and Pacific Oceans. In those areas, little confidence can be placed in the autocorrelation structure, but they are nevertheless presented for completeness.

In addition to the global 10^o grid, seven ocean-relevant areal averages of autocorrelation functions are presented. Those areas include: the Kuroshio subtropical gyre, 135°E-180°E,

25°N-40°N; eastern equatorial Pacific, 180°E-80°W, 10°S-10°N; northeast Pacific, 150°W-120°W, 30°N-50°N; East Australia gyre, 150°E-180°E, 40°S-10°S; Gulf Stream subtropical gyre, 80°W-50°W, 25°N-40°N; north Atlantic subpolar gyre, 60°W-10°W, 40°N-60°N; and the tropical Indian, 30°E-100°E, 20°S-10°N.

3. SPATIAL AUTOCORRELATION STRUCTURE

The lag autocorrelation function, AC(lag), is calculated as follows:

$$AC(lag) = \frac{\sum_{i=0}^{N-lag}(x_i - \bar{x})(x_{i+lag} - \bar{x})}{\sum_{i=0}^{N-lag}(x_i - \bar{x})^2}$$

where x is the measurement value and an overbar represents the average value. The spatial distance of the lag is simply the product of the index lag times the grid resolution between consecutive data points, in this case 2 km. For this study, we present results for an isotropic autocorrelation only, understanding that there are locations where the autocorrelation function is almost certainly not isotropic, near 40° - 45°N in the North Pacific, *e.g.* Murphy *et al.* (2001) performed identical calculations for 24 basin long repeat tracks of pCO_2 measurements made over a 48 months period along nearly great circle routes in the North Pacific. That study concentrated on the large scale spatial decorrelation estimates, and found that pCO_2 data became completely decorrelated (AC = 0) at about 1.5° longitude (105 km along the E-W direction) in the Bering Sea and 3.5° longitude (250 km along the NW- SE direction) in the Gulf of Alaska. In this study, it is the smaller scale variability that is of interest, and many data segments are not of sufficient length that would allow AC to approach 0.

Rather than presenting an estimate of the spatial autocorrelation function for each grid box, the global structure is presented as the lag distance at which the autocorrelation

estimate drops below a specific value. The first map (Fig. 3a) indicates the distance over which the autocorrelation is termed high, here, greater or equal to 0.8. The second map is the distance over which the autocorrelation is termed elevated, 0.6. These definitions of high and elevated are arbitrary, but nevertheless convenient for discussion purposes. The statistical significance of each autocorrelation is a function proportional to the number of data points that enter into the calculation of AC and varies geographically in this study (see Fig. 2). The globally recognizable feature is that the lag distance is shorter in high latitude areas and increases toward the equator, consistent with the dependence of the Rossby radius of deformation on the inverse of the local Coriolis acceleration.

The largest area where high autocorrelations extend to the greatest distance is in the immediate vicinity of the equatorial Pacific where that distance is routinely greater than 80 km, ranging from 100 km to 250 km in thermocline waters. There is some indication this "high correlation distance" is greater north of the equator than it is to the south in the Pacific Ocean. In the Atlantic, the high correlation distance is greater north of the equator than it is directly on the equator. In the Indian Ocean, the high correlation distance is greater south of the equator than it is to the north of the equator. The asymmetry in the Indian Ocean may be due to the long annual Rossby waves that dominate much of the variability in the southern Indian Ocean but does not in the north.

In the northern hemisphere subtropical gyres, the distance is greater (about 50 km) in the Atlantic compared to the Pacific where the distance is below 30 km. This distribution would be consistent with the eddy transfer scales in these gyres as the internal deformation radius of the subtropical gyre in the Atlantic is about 45 km, and that deformation radius is about 25 km in the Pacific (see Emery *et al.*, 1983 for estimates of deformation radii

based on local vertical Brunt-Vaissälä profiles). At high latitudes, the high correlation distance is 20 km and shorter, consistent again with the smaller deformation radii at these latitudes. Thus, in general, the distance for autocorrelations greater than 0.8 is consistent with scales set by the physical properties of the ocean flow in many areas.

Not surprisingly, there are aspects of the elevated autocorrelation distance (Fig. 3b) that are similar to the patterns of high correlation distance. For example, the longest distance for elevated autocorrelations is in the equatorial Pacific. Also, there are longer distances for elevated autocorrelation in the Gulf Stream gyre compared to the Kuroshio subtropical gyre are as in the high correlation distance pattern. However, there are areas in the high latitudes that have elevated autocorrelation distance that are comparable to the distances in the subtropics. This is somewhat evident in both the North Atlantic and North Pacific, indicating the autocorrelation function does not have a steep drop between 0.8 and 0.6 in those areas. Also note that the distances with elevated correlation are longer in the Gulf of Alaska compared to those east of the dateline at the same latitude consistent with the calculations of Murphy *et al.* (2001).

It is worth noting that even though the Murphy *et al.* (2001) study and this study used differing resolutions for the input data (10 km vs 2 km for the present study), both studies seemingly arrive at the same lag distance over which the autocorrelation drops below 0.8 in the northern North Pacific, about 20-40 km. However, the same zonal asymmetry appearing in both studies is a little surprising. The data used by Murphy *et al.* (2001) for the northernmost tracks between 170°E and 165°W were restricted within the Bering Sea, and the pCO_2 variability may likely reflect local turbulence generated by the Aleutian Island chain. In contrast, the variability of the northern North Pacific in our study is

represented mainly by data south of the island chain in the open North Pacific. Here, the shortened autocorrelation scales seem more likely tied to the variability of the Kuroshio Extension and Oyashio as opposed to local island effects that may have been important in the analysis of Murphy *et al.* (2001).

Around the Antarctic Circumpolar Current, the situation is more complex and changes in the elevated autocorrelation distance often varies greatly in adjacent grid boxes. The variability in this region is controlled by a strongly meandering zonal flow. The spatial scale of the local variability is much smaller than the 10^o x 10^o box used in this study. Thus the Antarctic Circumpolar Current and its variability are very much under-sampled, and this may explain the strong box to box variability in the autocorrelation calculations presented here.

The same calculations were repeated, except that average autocorrelation structures were calculated for two seasons, March-August and September-February, when the sun is at maximum zenith in the northern and southern hemisphere, respectively. Except for a slight tendency for there to be longer autocorrelation distances in the subtropical gyres when the sun is at zenith in the local hemisphere, there is very little seasonal change with the calculated autocorrelation structure. The change in the subtropical gyres was not significant enough to warrant showing the figures for the seasonal changes. The rapid change in autocorrelation structure over relatively short distances near the Antarctic Circumpolar Current did not change with season. Thus, biology seems an unlikely candidate for a single controlling factor of this spatial behavior. This is consistent with the small seasonal amplitudes of pCO_2 observed in the 40°S-60°S zone suggesting that pCO_2 changes due to SST are largely compensated by changes in TCO_2 due to the biological utilization and

upwelling (Takahashi *et al.*, 2002). The highly variable current and wind forcing make it difficult to assign any one reason for such variability in this area of strong horizontal and vertical mixing.

Fig. 4 is the estimated autocorrelation structure for seven specific geographic areas defined in the DATA section of this manuscript. Along with the estimated structure, a least squares best fit exponential curve to the average autocorrelation function is given to provide an estimate of an exponential decay scale of this structure. As indicated by the 10^o x 10^o estimates, the equatorial Pacific has the longest exponential decay scale of about 139 km. Also, the Gulf Stream decorrelation scale is nearly double than that occurs near the Kuroshio. An unexpected result is the relatively long 92 km e-folding scale in the North Atlantic subpolar gyre. Note, however, that the drop off for the highest correlation scales is not represented well by the best fit line in this area and a simple exponential decay would be an obviously poor choice for a functional representation of the autocorrelation function. This is also the case in the East Australia current region. Nevertheless, the exponential estimate provides consistent, if overly simplistic, comparison for the regions.

4. TEMPORAL AUTOCORRELATION STRUCTURE

Within this pCO_2 database, there are but a few time series of sufficient length to conduct meaningful temporal autocorrelation analysis. The pCO_2 time series at Hydrostation "S" (32°10'N, 64°30'W) and Bermuda Atlantic Time Series Study (BATS) site (31°50'N, 64°10'W) (Bates *et al.* 1999) in the Sargasso Sea, did not contain an uninterrupted time series longer than a few days. Much of the temporal analysis previously done for OWS "P" used, at best, weekly averaged data. For example, Wong and Chan (1991) analyzed the seasonal variation of pCO_2 at OWS "P" using monthly and weekly averaged values

of pCO_2 and reported slightly higher values of pCO_2 during summer compared to winter. Here the emphasis is on detailed temporal autocorrelation structure.

The temporal autocorrelation structure for the 11 longest uninterrupted time series from OWS "P" are shown in Fig. 5. The 6-hourly reported data has been averaged to daily values to remove diurnal effects. All these time series are from the 1970's with the longest segment being 42 days during 1978. Others are as short as 10 days. The shorter segments obviously have less confidence associated with the estimated structure. Whereas there are instances where the autocorrelation coefficient remains relatively high after a 5-day lag, the longer decorrelation scales can really not be associated with any particular time of year. The last two structures for the summer of 1978 illustrate this point. Whereas for Julian days 171-200 during 1978 the autocorrelation coefficient at 5-day lag is about 0.6, immediately following for Julian days 202-212, the coefficient is near 0 between 2 and 3 day lags. From the data available, it is difficult to assign a general structure to the temporal autocorrelation structure of daily pCO_2, even for a particular season. It is possible that longer period averaging, say weekly or monthly, might produce more consistent autocorrelation structure, however, the available data can not support those calculations.

Because uninterrupted time series of oceanic pCO_2 are scarce, an attempt is made to use other variables as a proxy to estimate the pCO_2 correlation structure, specifically temperature because of the great sensitivity of pCO_2 to temperature. Boutin *et al.* (1999) and Cosca *et al.* (2003) found that some of the pCO_2 variability in the eastern equatorial Pacific could be explained by the variability in temperature. Here, the four time series with pCO_2 data for at least 30 uninterrupted days is used to investigate the co-variability

of pCO_2 with temperature and salinity. The four pCO_2 time series are shown in Fig. 6. As in Wong and Chan (1991), most of the values of pCO_2 are between 290 and 340 μatm. The exception occurred during the summer of 1976 when a likely mixing event dropped surface pCO_2 values to near 250 μatm. The temperature and salinity data for this period show no unusual behavior. Since no nutrient concentration data are available for this period, the low pCO_2 values cannot be attributed unequivocally to biological utilization of CO_2.

Rather than presenting a simple correlation, we choose to present the coherence spectra between the temperature and pCO_2 data. The data is detrended by removing a linear best fit line, likely removing most of any local seasonal signal. The estimate of coherence between variables is identical to unity except when smoothing is applied to the estimates of the auto and cross spectra. For this analysis, a simple Hanning smoother, where a spectral component is replaced with a weighted (1-2-1) average of its surrounding components, is applied. The coherence spectra for the four time periods between temperature and pCO_2 are shown in Fig. 7. The value of coherence being 1 at either side of the frequency extremes is due to no smoothing of the spectra at end points. The jaggedness in each of the coherence spectra is obvious. Whereas the 1976 and 1977 periods might indicate greater coherence at lower frequencies, the 1978 sequences do not. Except for the 1977 series, there is a local peak at 0.2 cycles per day that might indicate that pCO_2 variability is related to mixing forced by atmospheric synoptic variability. However, it is difficult to say that a clear picture of covariability between pCO_2 and temperature on any particular time scale. Although not presented, the results are no more clear for pCO_2 and salinity covariability than they are for pCO_2 and temperature covariability at OWS "P".

The seasonal variability of pCO_2 observed in the OWS "P" area is generally less than 30 μatm (with an exception of one event in the summer of 1976) as shown in Fig. 6. This is about 20% of 140 μatm that is expected from the 9 °C seasonal SST changes if no change in TCO_2 occurred ($\partial \ln pCO_2/\partial T = 0.0423\ ^{\circ}C^{-1}$). Takahashi *et al.* (2002) have shown that the temperature effect was largely cancelled by the biological drawdown of TCO_2 during spring through summer and by the upwelling of CO_2-rich deep waters during fall through winter. Hence, the CO_2 system in this area depends only weakly on the seawater temperature. This accounts for the highly variable coherence between pCO_2 and SST, and the 0.2 cpd peak which may represents the effects of wind-induced deep mixing events.

5. SUMMARY AND CONCLUSIONS

A global database containing mainly underway measurements of surface water pCO_2 is used to estimate the spatial autocorrelation structure on a 10^o latitude-longitude grid. Since the pCO_2 is a sensitive function of temperature and the total CO_2 concentration in seawater, which depends on biological utilization and upwelling of CO_2-rich subsurface waters, its variability reflects both physical as well as biological processes. The pCO_2 is more densely sampled in space and time in northern hemisphere than the southern hemisphere. The longest spatial correlations occur in the equatorial Pacific where the autocorrelations are above 0.8 out to distances between 80 – 100km. The other equatorial areas also have relatively long correlation scales compared to other areas of the globe. The north Atlantic subtropical gyre has spatial correlation scales that tend to be about double the correlation scales in the subtropical gyre associated with the Kuroshio. This geographic distribution is similar to the distribution of the values of the first baroclinic

Rossby radii of deformation as calculated by Emery *et al.* (1983), indicating that the physical properties of the flow field are a likely contributor to factors controlling the correlation scales. In the Indian Ocean, the correlation scales in the southern hemisphere tend to be longer than those in the northern hemisphere. A possible explanation for this variability can again be related to the controlling mechanisms of the flow field. An important mode for the southern Indian ocean variability stem from long annual Rossby waves that are generated on the eastern side of the basin and propagate westward. The northern half of the basin is much more reactive to the strong forcing of the monsoonal flows. The correlation scales tend to be shortest at higher latitudes, again consistent with the scales of the deformation radius, but there is an indication that after an initial steep drop off of the autocorrelation, there is a slowing of the drop off between 0.8 and 0.6 in the northern Atlantic.

An attempt to estimate the temporal correlation structure is made at the only geographic location with relatively long (longer than about 10 days) uninterrupted time series of pCO_2 data, OWS "P", in the eastern North Pacific. Eleven time series were used to calculate the correlation structure with highly variable results. Most of these time series indicated a significant drop in autocorrelation (0.5 and lower) after 1-2 days. Three of the time series contained a more gentle drop off in the temporal correlation, but after 5-days, the correlation was only about 0.5. There was no obvious seasonal dependence in the temporal autocorrelation structure. Indeed, two of the time series that were separated by a single day during the summer of 1978 produced a drastically different autocorrelation structure from each other.

The coherence of the geographic distribution of the spatial autocorrelation structures with physical properties of the flow, such as the internal Rossby radius of deformation, is encouraging. As assimilation models are contemplated for pCO_2, it is necessary to have confidence in an error covariance model for the data being ingested. An autocorrelation function provides a good start, and the fact some of the global variability can be related to other physical variables gives some hope that any analysis product will be of more use than the ingested data alone. However, the inability to estimate a temporal autocorrelation structure is troubling. Even at OWS "P" where time series data exists, a stable estimate of that correlation structure proved difficult. The situation may not be hopeless. The estimates of the spatial correlation structure ignored any time change along a particular track, yet those correlations remained high over long distances, which also means over a time period of more than a couple days. Although modeling studies may be useful as a first guess for estimating pCO_2 correlation structure, confident estimates will require more and targeted measurements over the entire globe.

Acknowledgments. This research was sponsored by the Carbon Cycle Science research initiative within NASA's Science Mission. This research was funded through NASA's Carbon Cycle Science program as announced in NRA-00-OES-08. Takahashi and Sutherland are supported through NASA grant, NAG 5-11357. We acknowledge the following groups of investigators who provided the data analyzed in this study; C. S. Wong (IOS/Canada), R. A. Feely (PMEL/NOAA), Rik Wanninkhof (AOML/NOAA), Y. Nojiri (NIES/Japan), N. Bates (BBSR/Bermuda), B. Tilbrook (CSIRO/Australia) and A. Watson (Univ. East Anglia/UK).

References

Bates, N. R., T. Takahashi, D. W. Chipman, and A. H. Knap, 1998. Variability of pCO_2 on diel to seasonal timescales in the Sargasso Sea near Bermuda. *J. Geophys. Res.*, **103,** 15567–15585.

Boutin, J., J. Etcheto, Y. Dandonneau, D. C. E. Bakker, R. A. Feely, H. Y. Inoue, M. Ishii, R. D. Ling, P. D. Nightingale, N. Metzl and R. Wanninkhof, 1999. Satellite sea surface temperature: a powerful tool for interpreting in situ pCO_2 measurements in the equatorial Pacific Ocean. *Tellus, Ser. B,* **51,** 490–508.

Cosca, C. E., R. A. Feely, J. Boutin, J. Etcheto, M. J. McPhaden, F. P. Chavez, and P. G. Strutton, 2003. Seasonal and interannual CO_2 fluxes for the central and eastern equatorial Pacific Ocean as determined from fCO_2- SST relationships. *J. Geophys. Res.,* **108,** 3278-3288.

Emery, W. J., W. G. Lee, and L. Magaard, 1984. Geographic and Seasonal Distributions of Brunt-Vaissälä Frequency and Rossby Radii in the North Pacific and North Atlantic. *J. Phys. Oceanogr.,* **12,** 528–537.

Feely, R. A., Wanninkhof, R., McGillis, W., M.-E. Carr and Cosca, C. E., 2004. Effects of wind speed and gas exchange parameterization on the air-sea CO_2 fluxes in the equatorial Pacific Ocean. *J. Geophys. Res.,* **109**, CO8S03,doi:10.1029/2003JC00189

Loukos, H., F. Vivier, P.P. Murphy, D.E. Harrison and C. Le Quéré, 2000: Interannual variability of Equatorial Pacific CO_2 from temperature and salinity data. *Geophys. Res. Let.,* **27**, 1735-1738.

Murphy, P.P., Y. Nojiri, D.E. Harrison and N.K. Larkin, 2001. Scales of variability for surface pCO_2 in the Gulf of Alaska and Bering Sea: toward a sampling strategy, *Geophys.*

Res. Let., **28**, 1047-1050.

Takahashi, T., Olafsson, J., Goddard, J., Chipman, D. W. and Sutherland, S. C., 1993. Seasonal variation of CO_2 and nutrients in the high-latitude surface oceans: A comparative study. *Global Biogeochemical Cycles,* **7**, 843- 878.

Takahashi, T., Feely, R. A., Weiss, R., Wanninkhof, R. H., Chipman, D. W., Sutherland, S. C. and Takahashi, T. T., 1997. Global air-sea flux of CO_2: an estimate based on measurements of sea-air pCO_2 difference, *Proc. National Acad. Sci.,* **94,** 8292–8299.

Takahashi, T., Sutherland, S. C., Sweeney, C., Poisson, A., Metzl, N., Tillbrook, B., Bates, N., Wanninkhof, R., Feely, R. A., Sabine, C., Olafsson, J. and Nojiri, Y., 2002. Global sea-air CO_2 flux based on climatological surface ocean pCO_2, and seasonal biological and temperature effects,*Deep-Sea Res. II,* **49,** 1601–1622.

Wong, C. S., and Y.-H. Chan, 1991. Temporal variations in the partial pressure and flux of CO_2 at ocean station P in the subarctic northeast pacific ocean. *Tellus* **43B**, 206–223.

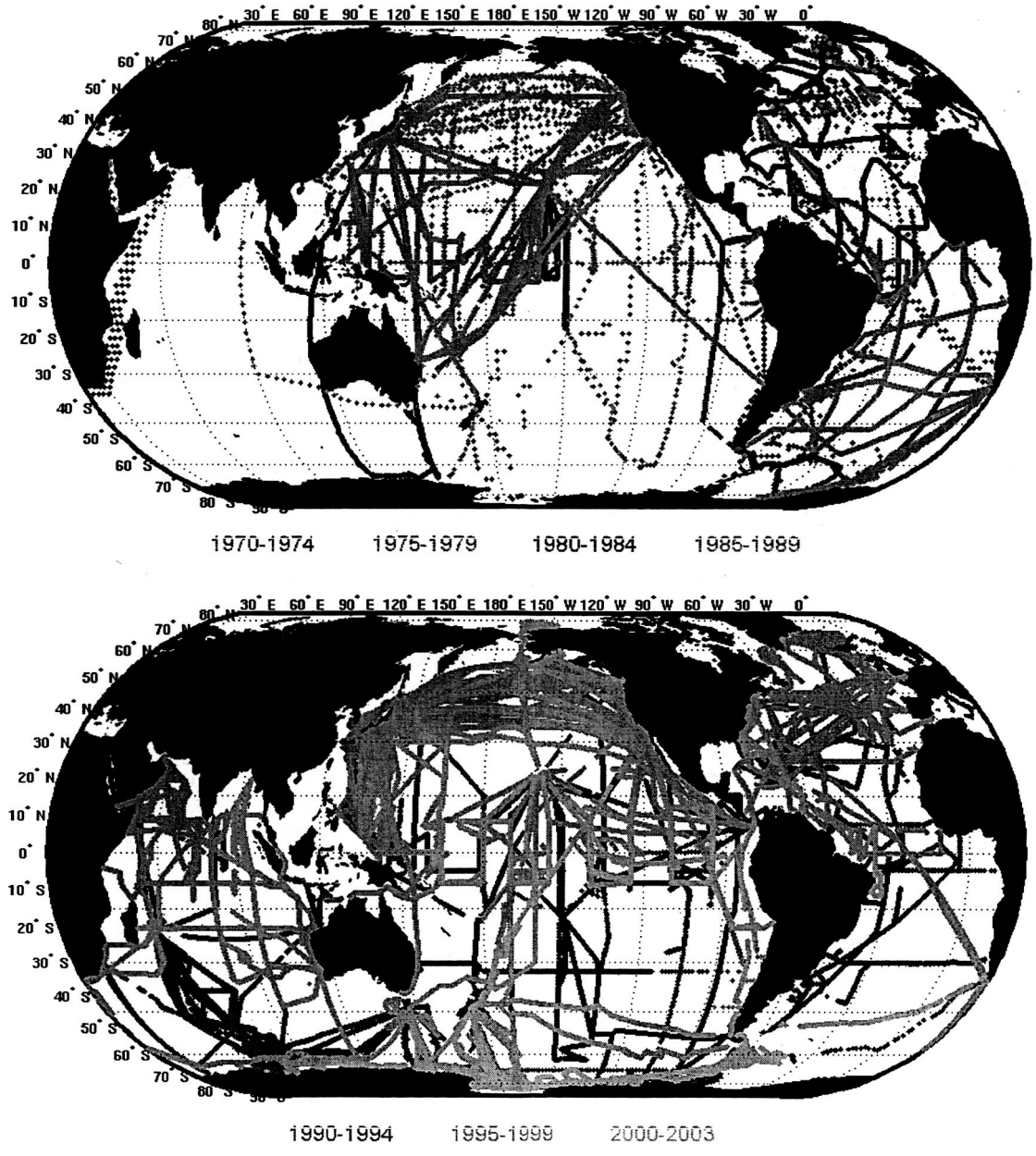

Figure 1. The spatial and temporal distributions of ocean surface pCO_2 measurements taken between 1970 and 2003. The location is marked on the map by a colored marker. The color of the marker indicates the pentad during which the observation was taken.

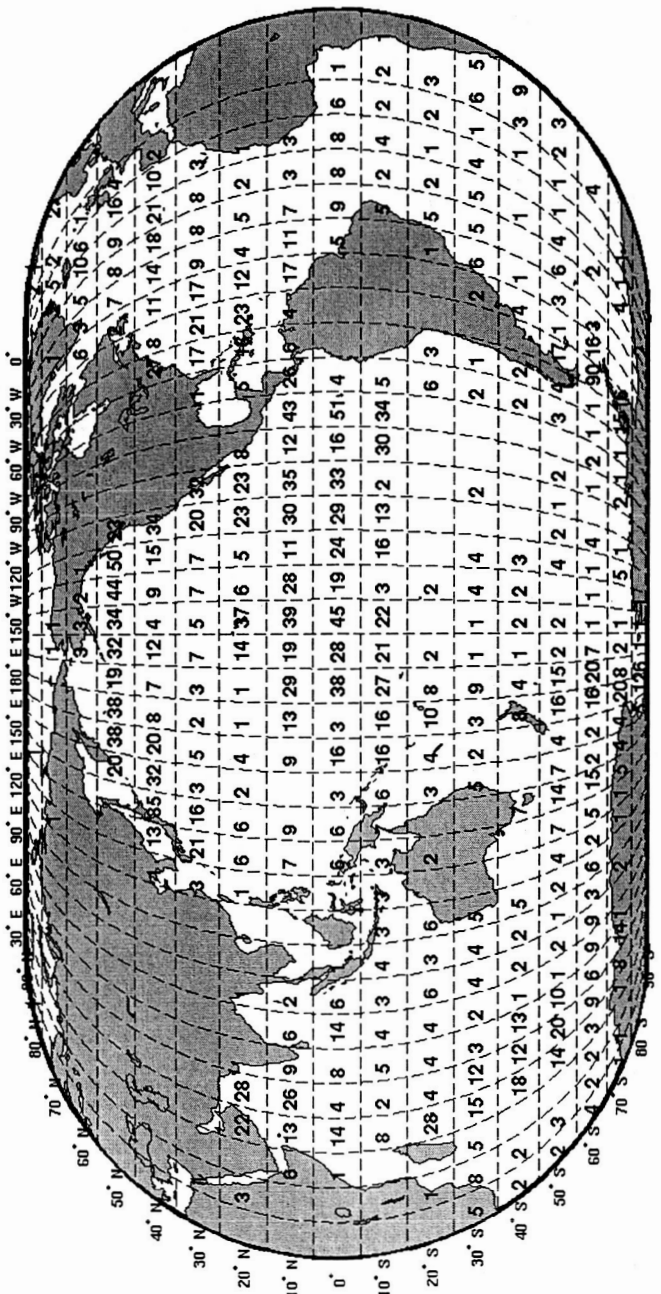

Figure 2. Distribution of the total number of defined pCO_2 measurement segments within each 10° x 10° box. Box colored white contain no pCO_2 measurements.

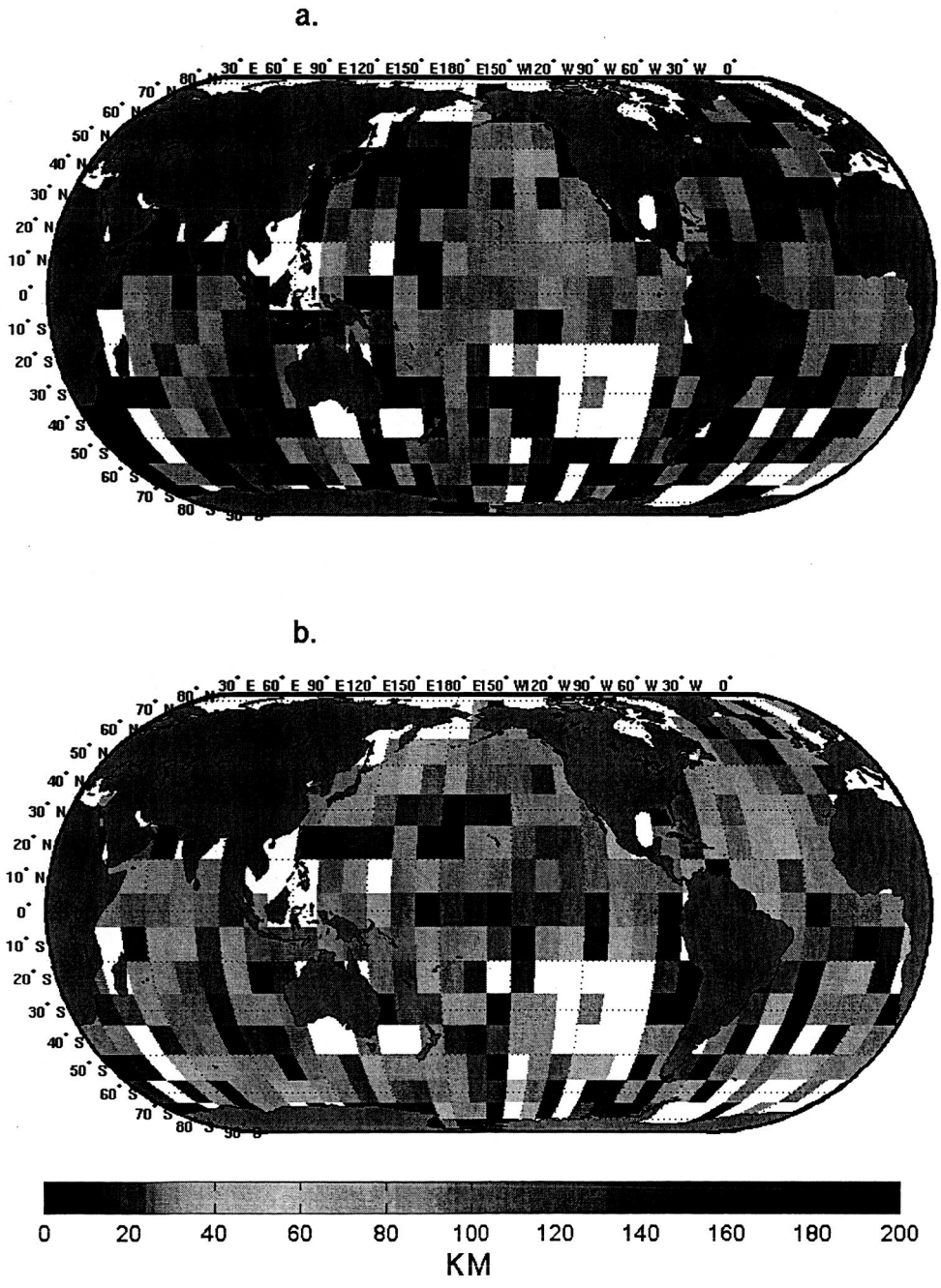

Figure 3. (a). Global distribution of lag distance where the spatial autocorrelation exceeds 0.8, and (b) the lag distance where the spatial autocorrelation exceeds 0.6.

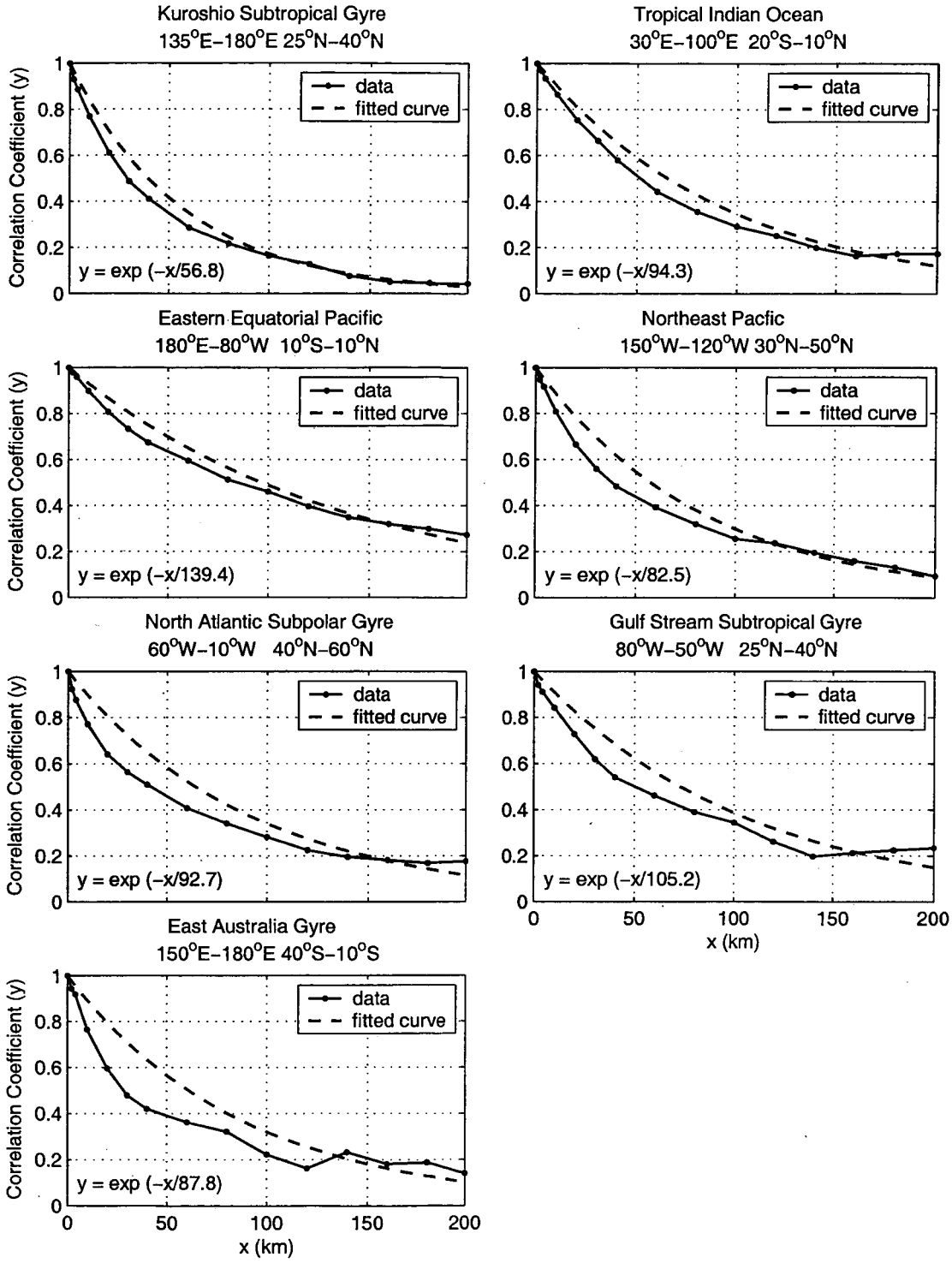

Figure 4. The estimated average spatial autocorrelation functions for seven specific geographic locations (solid lines with circles) and their best fits (dashed lines) assuming an exponential decay scale.

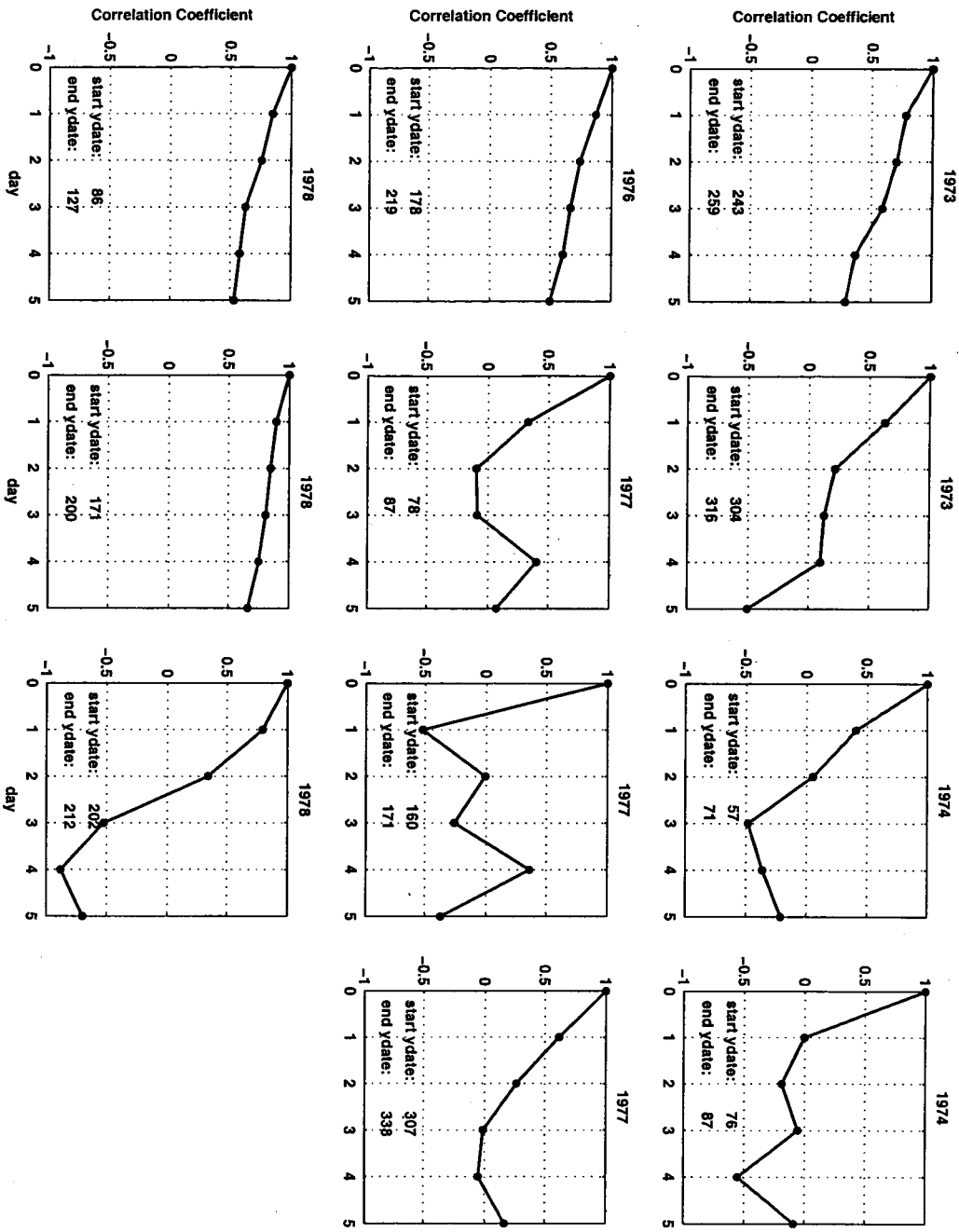

Figure 5. Estimates of the temporal autocorrelation structure for the 11 longest uninterrupted time series from Ocean Weather Station (OWS) "P" in the eastern subarctic Pacific ($50^oN, 145^oW$). The year of observation is shown above each plot, and the Julian Day of the beginning and end of each series is labeled within the plot.

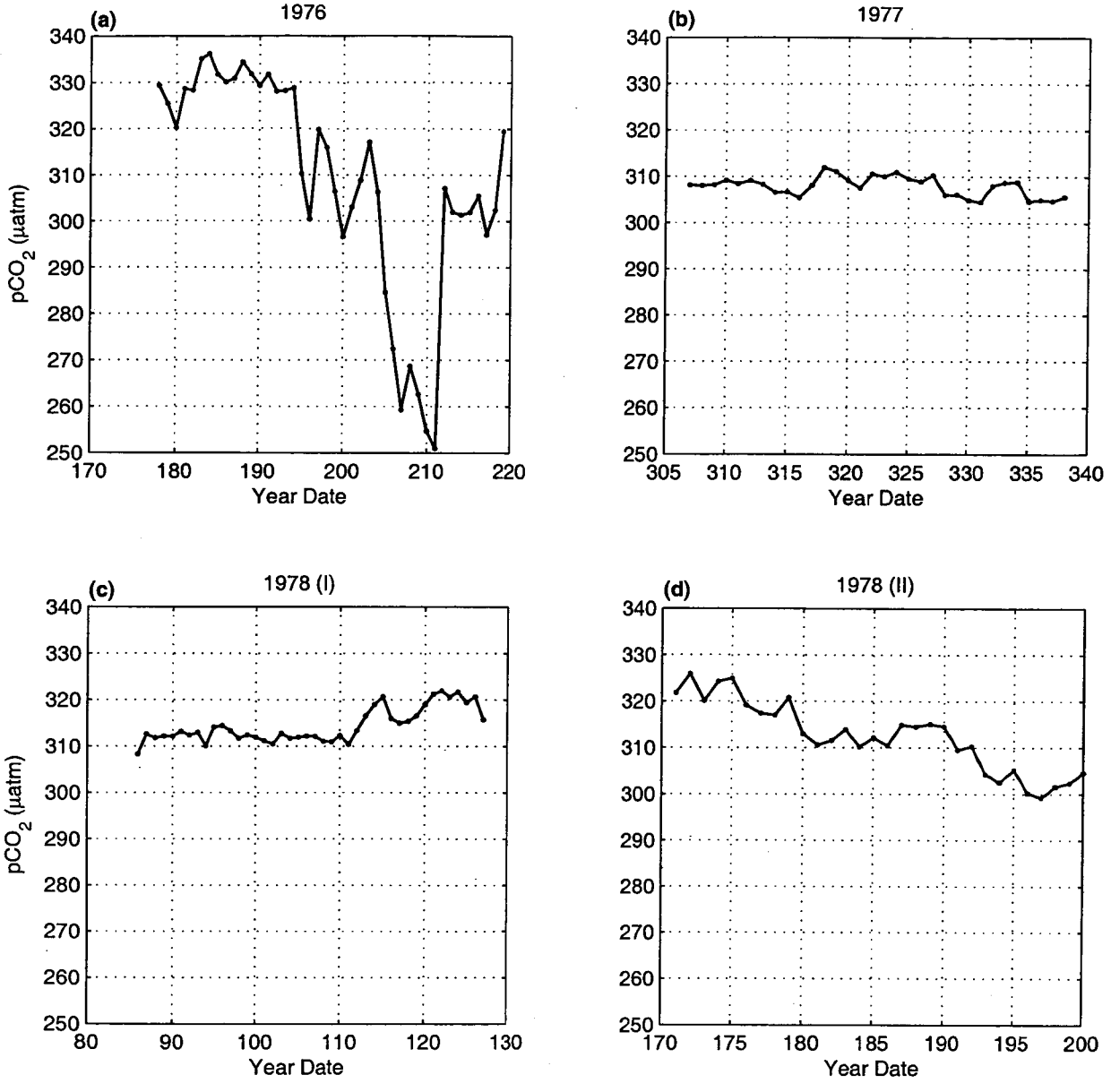

Figure 6. The four longest time series of daily averaged pCO_2 from Ocean Weather Station (OWS) "P" in the eastern subarctic Pacific (50°N, 145°W). These pCO_2 series are chosen for display because the length of each time series is at least 30 days. The year of observation is shown above each plot, and the Julian Day is marked on the abcissa.

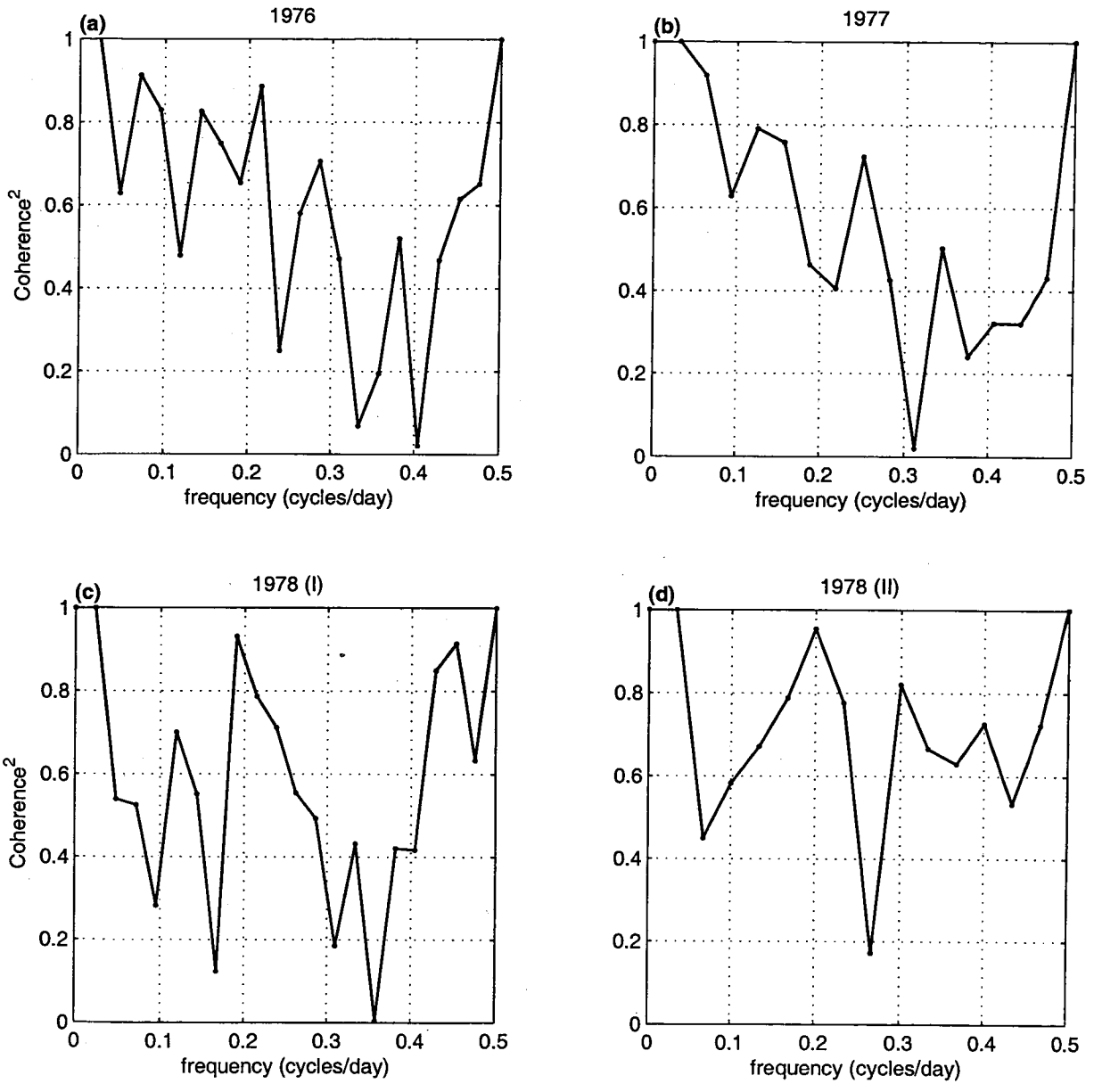

Figure 7. The coherence spectra between temperature and pCO_2 for the four time periods shown in Figure 6. The coherence was estimated using a Hanning (1-2-1) filter on the auto- and cross-spectral estimates.

POPULAR SUMMARY

Some variables related to climate are not currently observable from space and require in situ measurement. The dissolved CO2 in the surface water is such a variable and is important because it is a prime regulator of how much CO2 in the atmosphere is exchanged with the ocean. In this manuscript, the natural spatial scales of dissolved CO2 in the global surface ocean are identified. Knowledge of these scales is important as it helps determine the requirements for future measurements of CO2 variability in the ocean. This study clearly shows that the spatial scales of dissolved CO2 are intimately tied to the scales of the surface ocean circulation. The largest scales occur in the tropical Pacific, and shortest scales in polar regions. The estimates of these scales is also important for computer models and simulation of CO2 variability as these calculations provide the first global estimates of the finest spatial scales that models must resolve.

SIGNIFICANT FINDING

Although there have been a handful of studies documenting the observed scales of ocean surface CO2, this is the first study to present results of ocean CO2 scales for the entire globe.